EVALUATION OF SEISMIC CODE PROVISIONS USING STRONG-MOTION BUILDING RECORDS FROM THE 1994 NORTHRIDGE EARTHQUAKE

Juan C. De la Llera[1] and Anil K Chopra[2]

ABSTRACT

In this investigation the recorded motions in eight buildings obtained during the 1994 Northridge earthquake are studied and used to evaluate seismic code provisions and conventional building analysis techniques. These motions are first subjected to signal processing techniques to identify important building properties such as vibration periods and story stiffnesses. Then, the recorded ground motion in each building is used, in conjunction with a linear model of the structure, to predict the dynamic response of the building. Such response is then compared with the recorded response in order to assess the uncertainty present in the modeling procedure. Besides, a recently proposed improved inelastic model, based on the use of ultimate story shear and torque surfaces, is used to predict the response of buildings and explain conceptually their seismic behavior. Finally, instrumentation and code issues are discussed in light of the results generated in this research.

INTRODUCTION

The 1994 Northridge earthquake has produced one of the most valuable databases of ground and earthquake building responses in history. A total of 193 stations of the California Strong Motion Instrumentation Program recorded 116 free-field ground motions and 77 structural responses. From the latter, 57 correspond to buildings records obtained in a range of structural configurations.

The purpose of this investigation is to evaluate seismic code provisions using recorded motions in 8 buildings. In particular, the objectives are to: (1) evaluate current procedures for seismic analysis of structures; specifically, the uncertainty present in conventional structural building models; (2) evaluate deficiencies in current code provisions for earthquake analysis and design, and (3) propose improved analysis and design procedures calibrated using "measured" responses.

Because of the comprehensive nature of this study, this investigation has been subdivided into four phases. First, buildings records are studied and analyzed exhaustively to extract useful information of building properties and performance. Second, linear structural models are constructed for each building using conventional techniques. Third, improved, or state-of-the-art, structural models are developed to explain discrepancies in conventional linear models using nominal building properties. And fourth, improved code provisions are developed and calibrated using recorded building motions.

BUILDINGS CONSIDERED

The eight medium rise buildings considered in this study are listed in Table 1. They cover a wide range of typical structural systems in use today, such as R/C frames, precast R/C walls, R/C column-flat-slab frames, steel bracings, steel walls (uncommon), and mixed R/C and steel framing systems. Notice that for all these structures the peak ground accelerations during Northridge exceeded 0.2*g*. A brief description of each building is presented next.

[1] Department of Structural Engineering,, Catholic University of Chile

[2] Department of Civil Engineering, University of California at Berkeley

Building A

The building was designed in 1965, constructed in 1966, and is located 4.5 miles east of the epicenter aproximately. It is a nominally symmetric seven story R/C frame with approximate plan dimensions 62 x 150 feet. Its typical framing consists of columns spaced at 19 and 20 foot centers in the longitudinal and transverse directions, respectively., and spandrel beams run along the perimeter of the structure. The floor system consists of a 10 in. thick R/C slab at the second floor, 8 1/2 in. at the third to seventh floors, and 8 in. at the roof. The cylindrical strength of the concrete varies from 5 ksi and 4 ksi at the first and second stories to 3 ksi in upper stories. After the earthquake, the building was severely damaged on the longitudinal perimeter frames; damage also occurred on the E-W transversal frames but limited to minor flexural cracks in the end bays.

Table 1 Buildings considered

CSMIP Station	Building	Number of Stories	System	PGA x-direction	PGA y-direction
24386	**A**: Van Nuys (hotel)	7	R/C frame	0.44g	0.37g
24514	**B**: Sylmar (hospital)	6	R/C and steel frame and walls	0.52g	0.67g
24231	**C**: UCLA (Math-Science)	7	R/C walls and steel frame	0.25g	0.29g
24332	**D**: LA (commercial)	3/2[3]	Braced frame	0.33g	0.32g
24385	**E**: Burbank (residential)	10	R/C precast walls	0.27g	0.29g
24370	**F**: Burbank (commercial)	6	Steel frame	0.25g	0.29g
24652	**G**: LA (office)	5/1	Braced frame	0.24g	0.20g
24463	**H**: LA (warehouse)	5/1	R/C frame-flat slab	0.20g	0.26g

Building B

The building was designed in 1976 and its construction finished in 1986. Its lower two stories have a rectangular shape of approximate dimensions 302 x 452 feet; the upper four stories are cross-shaped with external dimensions 101 x 302 feet. The lateral force resisting system consists of R/C walls in the lower two stories and steel shear walls stories running along the 12 edges of the cross-shaped configuration in the upper stories. The floor system is composed of a corrugated steel deck and a 6" LWC slab. Only nonstructural damage to roof piping and chillers has been documented after the earthquake. This nonstructural damage is consistent with the high level accelerations (over 2g) recorded at the roof of the structure.

Building C

The building has a rectangular plan with dimensions 48 x 60 feet and was designed in 1969. The lateral resisting system in the first two stories consists of R/C walls, which enclose a nuclear reactor, and steel moment resisting frames in upper stories. The floor system is composed of a 2.5" floor slab over a corrugated steel deck at floors 4 through 8 and a thicker R/C slab on the third floor. No damage was reported in this building after the earthquake.

[3] n/m denotes n and m stories over and under ground level, respectively

Building D

This building was designed in 1974 and its construction finished in 1976. The two underground levels have a rectangular plan of dimensions 227 x 519 feet and a lateral resisting system consisting of 18" thick R/C shear walls running along the perimeter, 24" circular columns in the interior, and a 4.5" waffle slab with 14" beams. In the upper three stories the framing system consists of steel braced frames along the perimeter of the structure. The typical plan dimension for these stories is 219 x 241 feet; the floor system consists of a 3.5" LWC slab over a steel corrugated deck. No damage was reported on this building after the earthquake.

Building E

This ten story building was designed and constructed in 1974. It has a rectangular plan with dimensions 75 x 215 feet. Its lateral resisting system consists of precast concrete walls in both directions. The precast walls were fabricated using normal weight concrete with a cylindrical strength of 5 ksi. A wire mesh ASTM A185-61T of size 4"x4" (#4x#4) was used in all panels. Further, grade 60 reinforcing steel is specified in all drawings. The vertical load carrying system consists of precast and poured in place LWC slabs tied together with prestressing strands and supported by the laterally resisting walls. The foundation system is formed by 202 NWC piles 25' to 35' deep. No damage was reported on the building after the earthquake.

Building F

This six story steel building was designed in 1976 and constructed in 1977. It has a square plan of 120 x 120 feet. The lateral resisting system is formed by a perimeter moment resisting steel frame; the specified structural steel is A-36. All other interior frames are intended to carry only gravity loads. The floor decking system is formed by a corrugated steel deck filled with LWC (3" slab). The foundation system consists of 76 NWC piles 32 feet deep approximately. No damage was reported on the building after the earthquake.

Building G

This steel building was designed in 1988 and constructed in 1989. It has a square plan of 94 x 94 feet with four adjoined rectangular towers in each of the building corners. Each of these towers have Chevron type steel braced frames and moment resisting frames in two of their faces, respectively. A-36 steel is specified for all structural members with the exception of rigid frame columns which are ASTM-572, grade 50. Lateral resistance in the building is provided by these towers since all interior structural elements are intended to carry gravitational loads only. A 1 foot thick mat foundation is used under each tower and spread foundations are used for interior columns. No damage has been reported in the building after the earthquake.

Building H

This building is a five-story plus basement warehouse 280 x 361 feet in plan and was designed in accordance with the 1970 Los Angeles building code. The lateral resisting system consists of a ductile R/C frame along the building perimeter. An interior 6" flat-slab column system was designed to carry vertical loads only. The foundation system is formed by spread footings. No damage was reported after the earthquake.

ANALYSIS OF BUILDING RECORDS

The first task was to use techniques of signal processing, system identification and procedures alike to infer as much building information as possible from records without introducing strong modeling assumptions. Shown in Figure 1 is the flow of the eleven tasks considered for the analysis of building records.

First, the records were transformed into MATLAB [1] readable format in order to be processed within this computational environment. Once in MATLAB, the integrated building displacements were used to

interpolate deformations in those floors where no instruments were present. A cubic spline interpolation procedure was used to preserve not only the values of displacement at recorded floors but also smooth trends in the deformed shape of the building. Given the absolute displacements in the interpolated floors, their absolute accelerations were computed by differentiation of the displacements. These accelerations were then low-passed filtered by using a filter calibrated by recorded accelerations on instrumented floors. By using these accelerations, spectral analysis, time-frequency analysis and parametric identifications were performed to estimate the natural vibration frequencies of the building and possible nonlinearities of the buildings response. Besides, by assuming the building masses as known, story shear and torque plots were constructed (these plots are used later to characterize the behavior of the structure). Finally, empirical force displacement relationships were computed for each building story.

Because of the large amount of information generated in this task, it would be impractical to reproduce all results obtained. Hence, only few typical results are presented as examples of the methodology used. The reader is referred to [2] for more detailed information in all buildings.

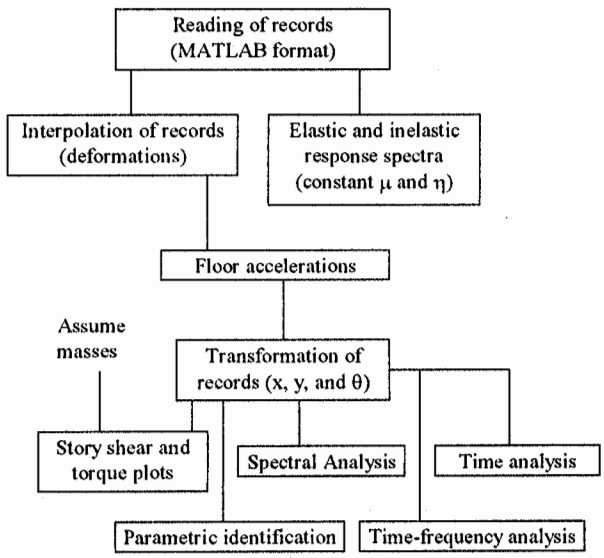

Spectral Analysis

Empirical transfer functions were determined with the purpose of estimating the fundamental building frequencies. These transfer functions were computed using Welch's method for spectral estimation [1]. Shown in Figure 2 is the result of spectral analysis, in this case for the records of Building F. The building frequencies are apparent from this figure; however, such is not always the case for other stiffer buildings. In this case the fundamental periods of the system are fx=0.68 Hz, fy=0.73 Hz, and 1.12 Hz .

Time-frequency analysis

In time frequency analysis a record is divided into overlapping segments and for each the power spectrum of the signal computed. This enables us to observe if the building properties vary in time because of nonlinearities in the structure. As an example consider the time frequency analysis of the records of Building A obtained during the San Fernando, Whittier, Landers, Big Bear, and Northridge earthquakes presented in Figure 3. In this figure the abscissa represents the central time of the segment of record considered and the ordinates the frequency ordering number. It is documented that Building A underwent some minor structural damage during the San Fernando earthquake but no damage until Northridge.

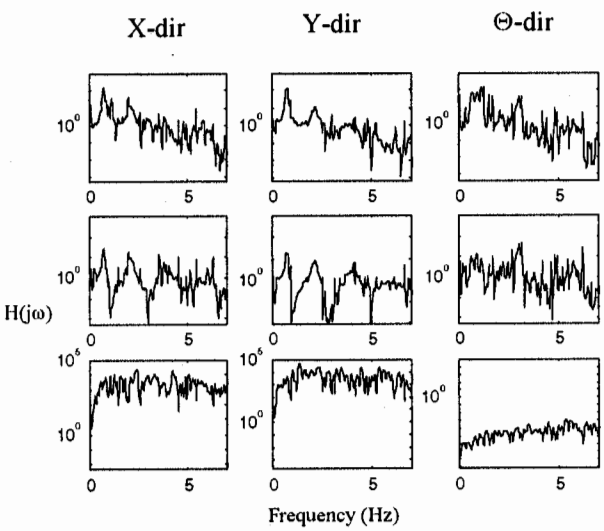

Figure 2 Transfer function of Building F accelerations

A careful examination of Figure 3 shows that the fundamental frequency of the building in the x-direction was f_x=0.68 Hz at the onset of the San

Fernando (1971) earthquake; this frequency was reduced to 0.58 Hz at the end of the earthquake, which is consistent with the observed structural damage in the building. Moreover, at the time of the Whittier (1987) earthquake, the building had increased its fundamental frequency to 0.88 Hz, probably because of the retrofit performed in the building after the San Fernando earthquake. During Whittier, the fundamental frequency of the building remained constant, implying elastic behavior of the structure. The same frequency is observed at the onset of the Landers (1991) earthquake; however, during the earthquake the building reduced again its fundamental frequency to 0.68 Hz, which was increased to 0.78 Hz, corresponding to the small amplitude vibration frequency, at the end of the record. This suggests that the building underwent some structural or nonstructural damage (or both) during Landers. Essentially no variation of frequency is observed during the Big Bear earthquake. Finally, at the beginning of Northridge the structure has a fundamental frequency of 0.64 Hz, similar to the minimum frequency obtained during Landers. This frequency is dramatically reduced to 0.44 Hz during the first twenty seconds of response; thus, justifying the damaged observed. Again, a small increase of this frequency to 0.54 Hz is observed toward the end of the record.

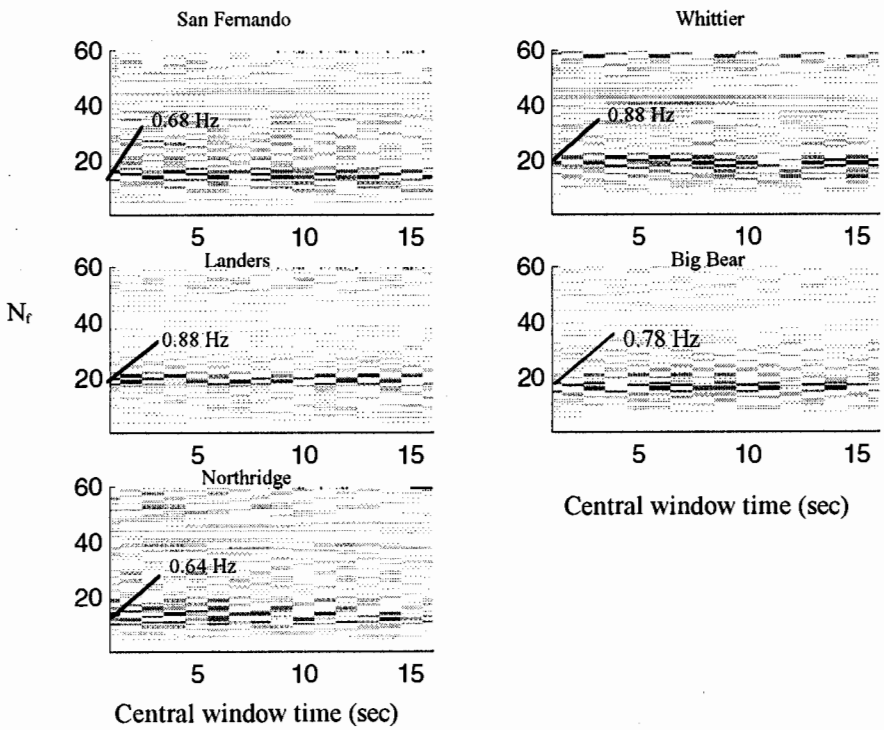

Figure 3 Time frequency analysis Building A

Following similar procedures to the ones already described, the natural periods of the other buildings considered were estimated. The results are summarized in Table 2 for six of the buildings considered. Presented in this table are also the torsional to lateral frequency ratios, $\Omega=f_\theta/f_x$, used later in the evaluation of accidental torsion

Table 2 Measured vibration periods

Building	T_x (sec)	T_y(sec)	T_θ(sec)	Ω_x	Ω_y
A	2.17	1.92	1.45	1.50	1.32
B	0.33	0.41	0.25	1.32	1.64
D	055	0.51	0.28	1.96	1.82
E	0.69	0.58	0.72	0.96	0.81
F	1.46	1.37	0.89	1.64	1.54
H	1.52	1.37	1.11	1.37	1.23

effects. As shown in this table, several of the buildings considered have closely spaced periods in the x and y directions of analysis.

Story Shears and Torques

This investigation uses extensively a recently developed structural building model that considers a single element per building story. The inelastic properties of such model are defined in the space defined by the story shears and torque. Consequently, the study of the building response in this space is of primary importance. Shown in Figure 4, for instance, are the story shears and torques generated in Building A during Northridge; these values have been computed assuming nominal values for the floor masses. For simplicity, results are presented only in the two dimensions defined by the x-direction story shear V_x and torque T. Each cross symbol plotted in this figure corresponds to a combination of story shear and torque for a different instant of time.

It is apparent from the figure, especially in the third, fourth, and fifth stories, that several story shear and torque combinations reach the same maximum value of shear, implying that there must be a surface (or region) beyond which these combinations cannot go. Such region is denoted as the story shear and torque surface and will be introduced later. Such surface will provide an interpretation to the story shear and torque combinations in terms of the behavior of the system.

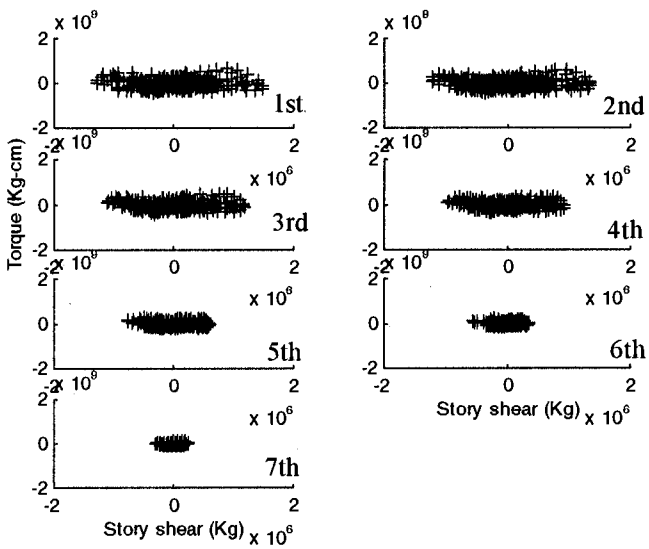

Figure 4 Story shears and torque (Building A)

Building deformations and story force-deformation relations

Because of the direct correlation between building damage and building deformations, the latter as well as the interstory drifts were computed for all buildings. Shown in Figure 5 are the deformations of the roof of Building E relative to the ground. Note that these deformations were computed subtracting the "true" absolute roof displacements from the ground displacements.

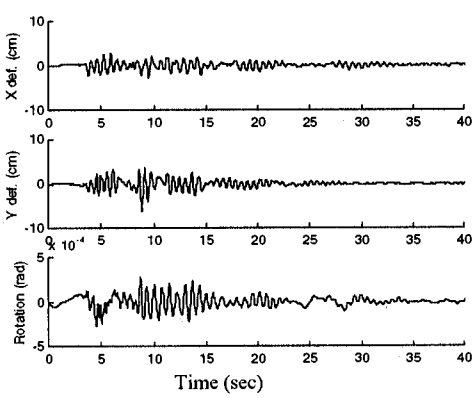

Figure 5 Roof deformations (Building E)

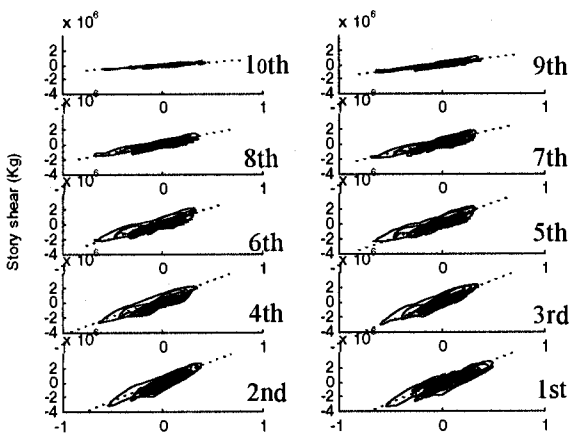

Figure 6 Story shear vs. deformation (Building E)

Using the story shears and torques computed in the previous section together with the interstory deformations of the building, the force deformation relations for each building story were computed. They are presented in Figure 6 for the longitudinal direction of the building. These curves assume, among other things, that the interstory deformations are due primarily to shearing of the story rather than rotation of the building underneath the story considered; an assumption that seems appropriate only for squat structures. Hence, strictly, they are only rough estimators of the true force-deformation characteristics of the building. In spite of this, we will see they provide a good insight on the relative story stiffnesses.

BUILDING MODELS

The objective of this phase is to assess the uncertainty present in building models as used in practice. For that purpose, the dynamic response of full three dimensional finite element models of the buildings considered are computed and compared against the measured response in them during the earthquake. The building responses are obtained assuming in-plane rigid floor diaphragms and three degrees of freedom at the center of mass (CM) of each floor, where all the story masses are lumped. Next, a brief description of the building models is presented together with the most important considerations and assumptions in their development.

Building A

Shown in Figure 7 is the structural model constructed for Building A. The model has 295 nodes and 665 elements and has been assumed fixed at the base level. Because of possible R/C cracking due to gravitational loads, the flexural stiffness of spandrel and interior beams has been reduced by half; this reduction has been considered in the model by ignoring the contribution of the slab in the flexural stiffness of beams.

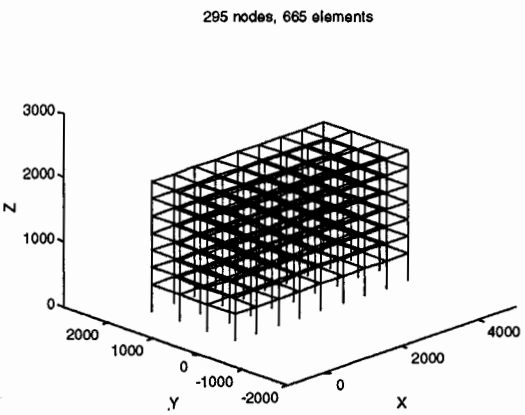

Figure 7 Structural model of Building A

Shown in Figure 8 is the estimated deformation (relative to the base) of the building roof when subjected to the true excitations at the base. For comparison, the true roof deformation is also presented in the figure. It is apparent that the estimated roof deformation using the linear model is substantially different from the true response. A probable explanation for this is the nonlinear behavior of the structure which is not accounted for in the linear model. This can be easily checked by noting that the estimated traces of the roof deformation are similar to the true deformations during the first four and eight seconds of the record in the x- and y-directions, respectively, and then become substantially different. Linear models are common practice in building analysis today in spite of the well known fact that buildings behave inelastically during strong earthquakes.

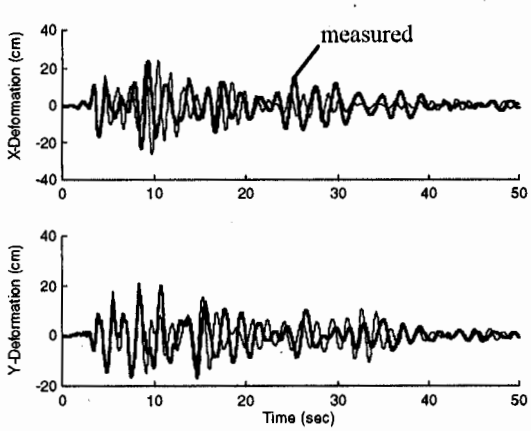

Figure 8 Estimated and 'true' deformations, Building A

Building B

Shown in Figure 9 is the structural model of the upper three stories of Building B. The

lower two stories were modeled using and empirical linear model obtained from the force-deformation story laws shown earlier (e.g.,Figure 6, for Building E). The purpose of this was to isolate the uncertainty in the modeling of the steel shear walls of the structure. The properties of these walls were computed discretizing in layers the walls in height to include the openings in them and then restoring, using basic beam theory, kinematic compatibility at the interface of each layer. This was done for shear as well as flexural deformations. In total, the model considers 730 nodes and 964 elements.

The comparison between estimated and 'true' deformations is presented in Figure 10. Although the estimated building frequencies are closed to those of the real building, the traces show important differences, especially in the x-direction. These discrepancies cannot be attributed to nonlinear behavior of the structure as for Building A since we know the building performed elastically. Rather, they probably come, in great proportion, from stiffness modeling uncertainty. Note, however, that the traces of 'true' deformation show trends at certain instants that are not physical (see, for instance, the linear trend at the initial four seconds of response). Therefore, it would incorrect to attribute all errors to structural modeling.

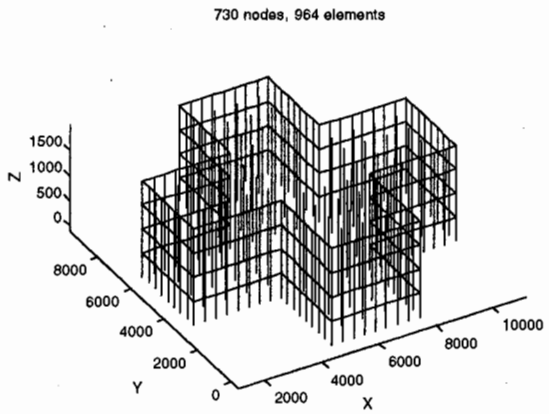

Figure 9 Structural model of Building B

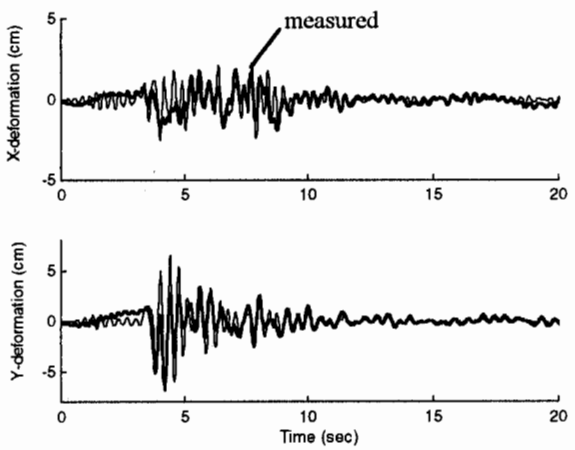

Figure 10 Estimated and 'true' deformations, Building B

Building D

The structural model of this building considers 805 nodes and 1675 elements (Figure 11). Both, the steel bracing structure and framing system of the upper three stories as well as the R/C column-flat-slab system of the lower two stories are included in the model. Such is the case because two other buildings rest on the same column-flat slab system and, hence, interaction with the neighbor structures occurs through the lower two stories. Besides, interstory secondary bracing elements, intended to reduce the effective length of the principal braces, were also included in the model.

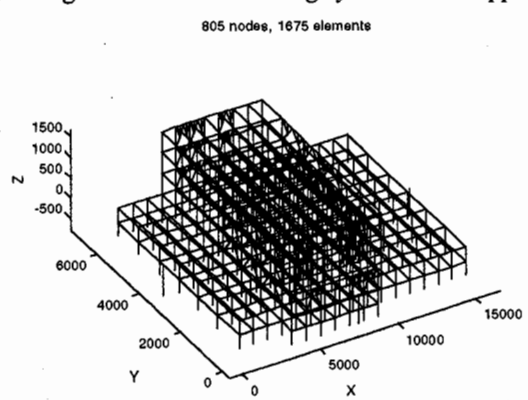

Figure 11 Structural model of Building D

Shown in Figure 12 are the roof deformations estimated using the building model and the actual deformations of the roof computed from building records. The responses have certain similarity in their frequency content but otherwise the response histories are different. Indeed, they are relatively similar only in the first few seconds in spite of the

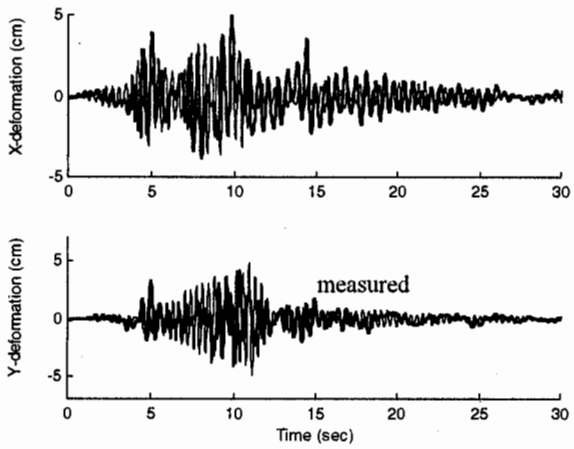

Figure 12 Estimated and 'true' roof deformation, Building D

tremendous effort done to model this structure accurately.

Building E

The model of this building is shown in Figure 13. It considers 1242 nodes and 2090 elements. Spring-like connection elements are used among R/C precast walls with the purpose of modeling the uncertain stiffness of these connections and their effect on the building response. The model presented herein, however, considers connections with zero stiffness as suggested by the details presented in the structural plans. Cracked properties, associated to the building dead loads, have been considered in defining the flexural stiffness of walls. Finally, the building model was considered fixed at the base of the first story.

The estimated and 'true' building deformations at the roof are presented in Figure 14. The figure shows that the estimated response contains slightly higher frequencies than the measured response. Moreover, the estimated deformations are consistently smaller than the measured ones. Such smaller vibration period could be due to soil structure interaction, as have been suggested by an earlier study on the building [3].

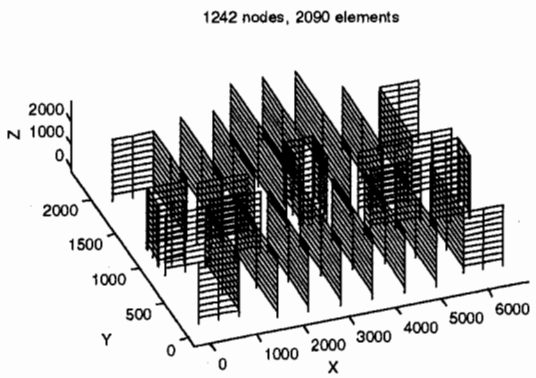

Figure 14 Structural model Building E

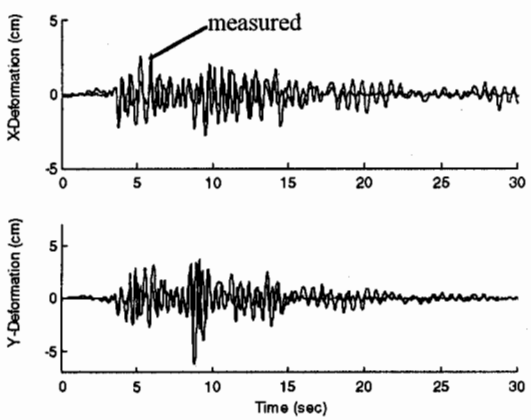

Figure 13 Estimated and 'true' roof deformation, Building E

Building F

The model for this six-story building is presented in Figure 15 and considers 349 nodes and 288 elements. The lateral resisting elements along the perimeter of the structure as well as all internal columns, intended to carry gravitational loads only, are considered in the structural model.

A comparison between the estimated and 'true' roof deformations is presented in Figure 16. The estimated response presents a predominant frequency that is slightly higher than that present in the 'true' building response. Apart from this difference both traces have amplitudes that differ considerably at certain instants and become closer at others, for instance, during the first ten seconds and trail of the record.

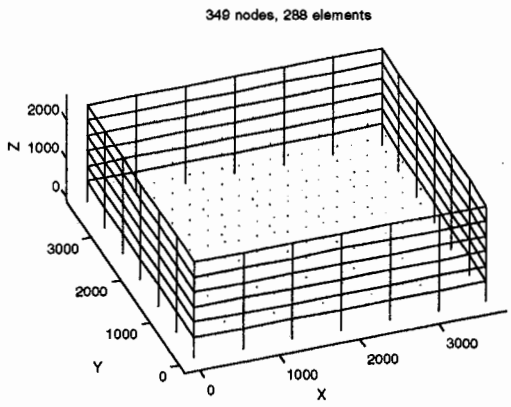

Figure 15 Structural model, Building F

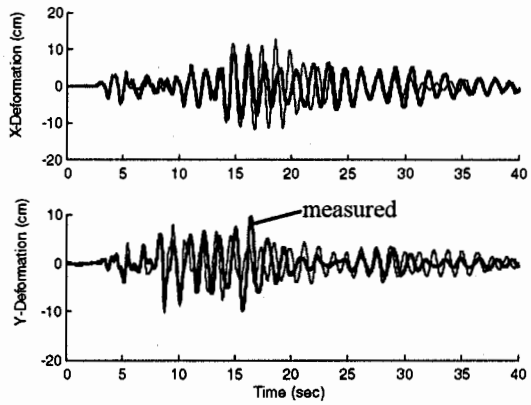

Figure 16 Estimated and 'true' roof deformations, Building F

It is important to note that any of the models presented could have been "touched up", even with physical considerations, to provide much closer estimates of the measured responses. However, as they are, they provide a good measure of the real model uncertainty that is present during the analysis process. In general, the estimated building responses using conventional modeling and analysis techniques provide trends that bear some resemblance with the measured responses. However, if the comparison is made in terms of peak responses they may differ typically in 30% to 50%.

IMPROVED ANALYSIS PROCEDURES

In this section a new procedure for building analysis that has been recently proposed by the authors is evaluated and tested using recorded building responses. For the sake of brevity, only the analysis of Building A will be presented in detail.

In the three-dimensional model developed, each story is represented by a single super-element (SEM) capable of representing accurately the elastic and inelastic properties of the story. The formulation of this model is described in [4] where its accuracy was tested using *theoretical* single and multistory systems. Besides, the model is based in the theory of plasticity and, hence, it assumes that the building develops plastic behavior (as opposed to sudden brittle behavior). Because Building A shows a brittle type failure in its columns along the perimeter, the use of the single-element model in this case goes a bit beyond its own scope. However, it will still provide good insight of the behavior of Building A during Northridge.

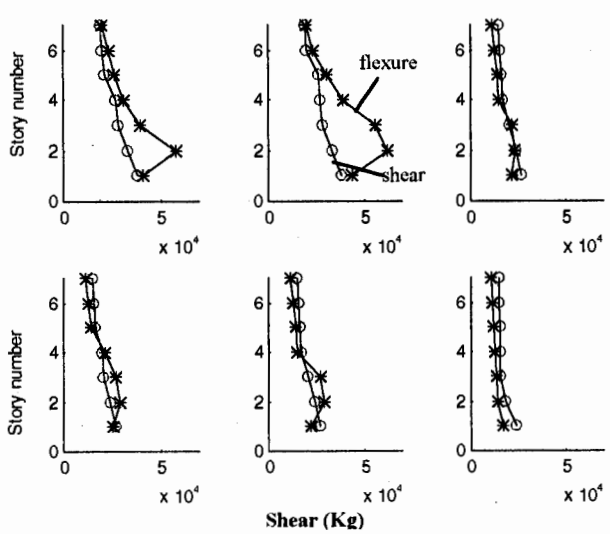

Figure 17a Column capacities in x-dir, Building A

The first step in computing the SEM for Building A requires to estimate the capacities of each story. This is done by first computing the lateral capacity of each building column corresponding to a meaningful axial load in the column. These loads were assumed in this case to be equal to the gravity loads. Shown in Figure 17 are the heightwise distribution of lateral capacities of the different types

of building columns.

The values identified with circles and stars correspond to lateral capacities associated to shear and flexural failure mechanisms in the column, respectively. It is interesting to note that for essentially all columns shear failure mechanisms control over flexural mechanisms in stories two through four, which were exactly those most severely damaged with shear-type mechanisms during the earthquake.

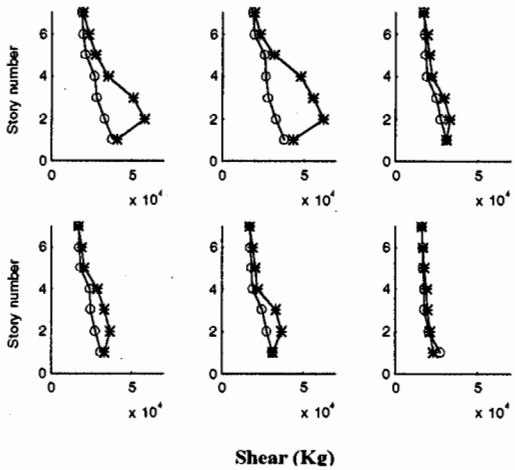

Figure 17b Column capacities y-dir, Building A

Using the column capacities presented above it is possible to construct a surface, denoted hereafter as story-shear and torque surface (SST), which bounds the dynamic response of each story of the building in the shear and torque space. Each point of this surface represents a static combination of story shear and torque that produces collapse of the story. Moreover, the different regions of this surface are associated to different story mechanisms. Recalling Figure 4, where the story shear and torque histories were introduced, it is possible to superimpose the theoretical SST on this plot as shown in Figure 18. Because the SST response histories must be bounded by the SST surface, it is apparent that we have underestimated the strength of the system in stories 1 through 5 (the upper two stories we cannot know since they are elastic).

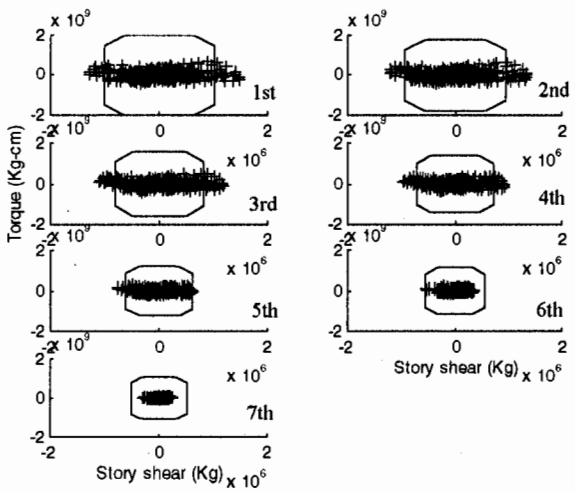

Figure 18 SST surfaces and histories

Therefore, two physically motivated corrections are applied to these surfaces. First, they are corrected for *overstrength,* defined as the ratio between the maximum measured story shear and the maximum estimated story shear capacity. Second, they are corrected for the effect of the orthogonal component of ground motion as proposed in [4]. Shown in Figure 19 is the result of these two corrections.

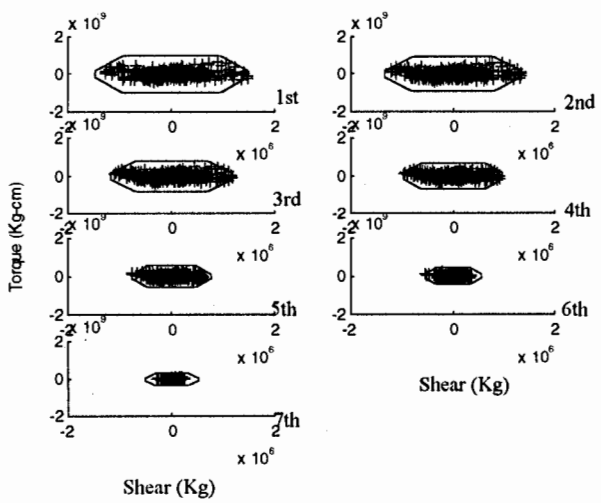

Figure 19a Corrected SST surfaces

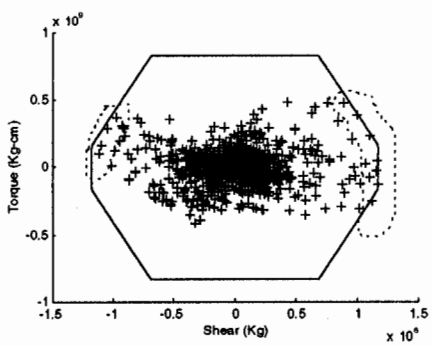

Figure 19b SST surface of third story, Building A

Several interesting observations are obtained from Figure 19. First, it is apparent that all the response shear and torque combinations lie inside the boundaries of the theoretically computed SST. This is important because the only adjustment done to the results of Figure 18 was the overstrength scaling based only on the peak story shear at each story. Second, Figure 19b is remarkable in showing that there is a number of story shear and torque combinations that lie exactly on the SST; these combinations have been circled in the figure. This implies, unless a very unlikely coincidence, that the actual story shear and torque combinations associated to inelastic behavior of the story belong to the SST surface as assumed theoretically. This observation proves that the SST model is in agreement with the actual behavior of buildings. Moreover, the story shear and torque combinations lying on the inclined branches of the surface indicate that the building underwent inelastic torsional behavior in spite of its nominal symmetry. Indeed, this will be the case in most buildings with perimeter frames as the only lateral resisting system. Finally, it is important to note that since there is only few points that reach the SST surface, i.e., few inelastic excursions of the story, the damage of the structure can be justified only if the ductility capacity of the system was small.

To verify this, shown in Figure 20 is the inelastic response spectra of the x-component of ground motion in Building A. According to the results presented earlier, this building has a capacity parameter $\eta=R_y/M$ $a_{max} = 0.94$, where R_y is the yield capacity of the building (in this case computed at the base), M the mass of the structure, and a_{max} the peak ground acceleration. Recognizing that the undamaged vibration period of the system is about 1.5 sec, the global ductility demand on this structure is slightly less than 1.1. This implies that although the structure was probably designed for target ductilities of, say, 6, its actual ductility capacity was close to one.

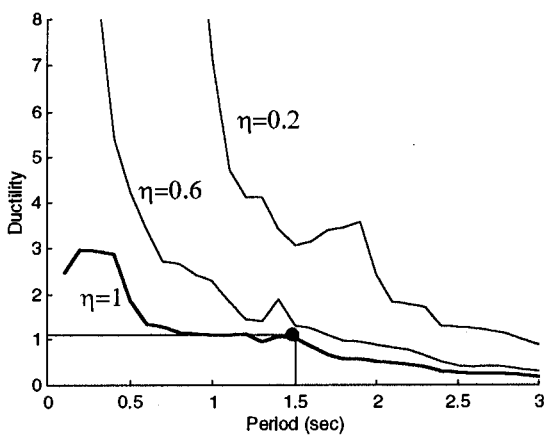

Figure 20 Inelastic response spectra, Building A

Finally, knowing the SST surfaces for each story, the SEM can be constructed an the inelastic response of the building predicted. Such response is presented in Figure 21. Although differences still exist between model and 'measured' responses they have been reduced relative to the elastic prediction shown earlier in Figure 8. It is also possible to show that since yielding in the structure is not substantial, an elastic model with stiffness reduced fits well the response. This confirms once again that Building A had a brittle behavior that could be modeled accurately by simply reducing the stiffness of the structure.

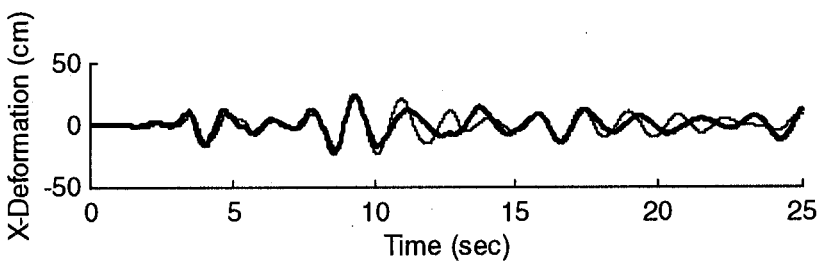

Figure 21 Estimated inelastic and 'true' building responses, Building A

INSTRUMENTATION AND BUILDING CODE IMPLICATIONS

In this section the results presented in the previous sections are used to address a number of instrumentation and code issues. The issues addressed are classified in the following groups: (1) instrumentation and record processing, (2) building modeling, (3) ductility of structures, (4) perimeter frame structural configurations, and (5) accidental torsion. For the sake of brevity, a full treatment of the ideas is not presented herein; rather, they are introduced briefly by showing examples and stating their implications for building analysis and design.

Instrumentation and record processing

A fundamental aspect of the investigation presented is to use recorded motions in buildings to the maximum extent possible without introducing strong modeling assumptions. However, is it possible to test fully our building codes and analysis procedures using only the recorded building information? Strictly speaking, the answer is no, unless all floor have been completely instrumented with at least three independent components; in such case we would be able to compute, for instance, the "true" interstory deformations, story shears and torques (if the masses are known), accidental torsion effects, etc. Such alternative, however, is not economically feasible except for very special buildings. This implies that the current "sparse" records in buildings must be somehow used to predict the motions of uninstrumented floors. Two alternative procedures can be used to do so: (1) system identification, and (2) record interpolation.

Record interpolation has two features that make it attractive. First, it is not restricted to a model structure as any identification procedure. For instance, if the building is linear and nonlinear at intermittent intervals the procedure is still valid. Second, it is simple to use and calibrate.

The interpolation procedure proposed considers first interpolation of the building deformations using cubic splines---cubic splines are truncated polynomials that possess continuity of slopes at interpolated points, and differentiation of the total interpolated displacements to estimate floor accelerations. A low-pass filter is designed, based on the recorded displacements and accelerations, to filter the resulting floor accelerations. Because building deformations are smoother functions they are preferable to accelerations for the interpolation procedure. An illustration of such procedure is presented in Figure 22, in which the recorded motions of Building A are used to estimate the displacements and recorded accelerations of the 6th floor. These predicted motions are compared against the recorded motions at the East end of the structure. The results show that the procedure can be quite accurate even for Building A which has a strong nonlinear behavior.

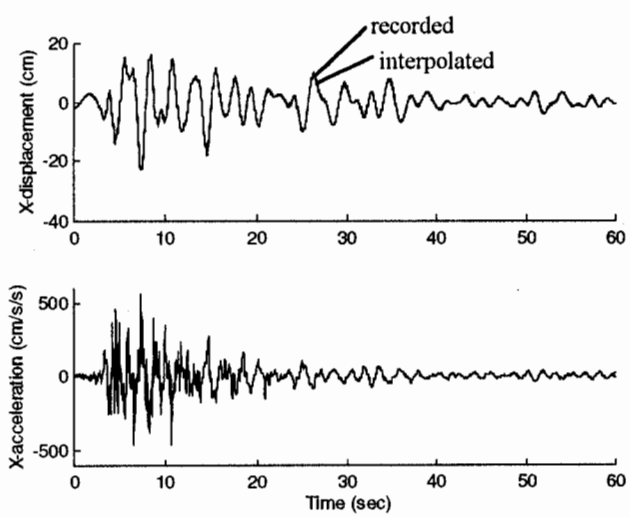

Figure 22 Exact and interpolated motions, Building A

Building modeling

In conventional studies of building records a model of the building is developed and subjected to the recorded ground motions. Frequently, such building model is then identified and adjusted in order to reproduce closely the recorded responses. It is an important question, however, how close was the response of the first model attempted relative to the recorded motions in the structure. That discrepancy or model uncertainty would have existed in the design of the structure in the absence of recorded information.

The results presented in Figures 8, 10, 12, 13 and 16 partially answer the question of model uncertainty. It is extremely hard to achieve better accuracy in practice using these conventional building models. It is apparent from these figures, however, that model uncertainty is highly correlated with the complexity of the structural system. Thus, the dynamic response predicted for Building F (Figure 16), which is essentially a clean perimeter frame, is much closer to the actual response than is for the complex structural plan of Building D (Figure 12).

Another important issue regarding structural modeling is the use of elastic models for building analysis and design. Although Building A (Figure 8) did not have substantial inelastic behavior, it seems inappropriate to use an elastic model to design this structure knowing, a priori, that the building is designed to experience substantial inelastic behavior during an earthquake like Northridge. This point is demonstrated by comparison of the elastic and inelastic building responses shown in Figures 8 and 21; indeed, the differences would be much more striking if the ductility demand on the building would have been larger.

A fundamental result of this investigation is the experimental verification (Figure 19) of the SEM (single element model) used for elastic and inelastic building analysis. This simplified model enables the engineer to compute the inelastic response of a building at a cost that is considerably smaller to that incurred in a full elastic three-dimensional analysis, with the advantage of capturing better the actual building response. Moreover, the use of the SST (story shear and torque surfaces) forces the engineer to understand the properties of the structure that control its inelastic behavior, thus, revealing any gross deficiencies in the planwise distribution of strength.

Ductility of structures

It is a widely accepted philosophy for earthquake resistant design that the capacity of a structure may be reduced if the system is able to accommodate in a *stable manner* larger deformations that surely imply damage in the structural elements. This philosophy is built in the reduction factor R_w present in most building codes; however, how can the engineer guarantee that the target design ductility values are achievable in the structure as built. Generally, it is argued that this is obtained through a good detailing but it should also be added a conceptually healthy structural configuration.

A good example of the lack of consistency between the assumed R_w in building analysis and the 'true' ductility capacity of a building is provided by Building A. According to current building codes a R/C ductile moment resisting frame could be designed for an R_w of 8 (up to 12), i.e., μ=6 (8), approximately. The ductility demand on Building A did not exceed 1.1 and, yet, the building collapsed. This is only possible if the building had a brittle behavior; thus, contradicting the initial design assumption of large deformation capacity.

Perimeter frame

Intimately related to the discussion above of building ductility is the issue of a conceptually healthy structural configuration. Several conditions characterize a good structural configuration: redundancy, capacity to generate uniform deformation demands in structural elements (regularity), and insensitivity to changes in the ground motion characteristics. A good example of redundancy is Building E in which damage of one element does not imply collapse of the system. In turn, a nominally symmetric systems, such as Building F, is a good example of a structure that generates (in theory) uniform displacement demands. Finally, insensitivity to ground motion characteristics is achieved by structures which confine the response in specific regions of the SST space.

The perimeter frame, as a structural concept, violates almost automatically the redundancy condition. Redundancy is violated because all columns at a given story and one edge of the building undergo simultaneously similar deformations and, hence, failure of one column signals, almost always, failure of all the other columns in the same resisting plane. A good example of such behavior is Building A, in which essentially all columns on the south perimeter resisting frame collapsed. This is because similar displacements are imposed by the rigid floor to all columns---a phenomenon similar to the one occurring

in piers supporting a rigid freeway deck. In general, plan redundancy is achieved primarily by more resisting planes and not by more structural elements on a resisting plane.

Besides the redundancy problem of perimeter frame configurations, they also have a serious deficiency in their inelastic behavior that can be visualized using the story shear and torque plots (e.g., Figure 19a and b). From this figure we observe that the building surfaces have three well defined slopes, one associated to constant story shear, one with a finite slope, and the last with constant story torque. The story shear and torques associated to the constant shear region correspond to story mechanisms that involve primarily translation and yielding of all resisting planes; the inclined branches are associated to mechanisms that leave the same perimeter frame elastic; and the constant torque regions involve mechanisms that are essentially torsional. As shown in Figure 19, most of the shear and torque combinations that touch the surface do it on the inclined branches. This implies that Building A, in spite of its nominal symmetry, develops mechanisms that involve important torsion, which in turn implies that one perimeter frame yields and damages while the other remains essentially elastic. This is exactly what happened in Building A where damage was localized more in the south resisting plane than in the north frame. The important observation is that perimeter frame systems will always tend to fail by predominantly torsional mechanisms which use inefficiently the capacity of both frames in the same direction localizing damage in one of them.

Accidental torsion

A new procedure to account for the increase in response due to accidental torsion has been recently proposed [4]. This procedure defines the increase in edge deformations due to different sources of accidental torsion such as stiffness and mass uncertainty and base rotational motion. Such procedure had been tested only with three nominally symmetric structures; however, four new cases: Buildings B, E, F and H can be added to this list. The results are presented in Figure 23, where Ω represents the ratio between uncoupled torsional and lateral frequencies, and the ordinates represent the ratio between the edge story deformation including rotation of the plan and without it. These deformation ratios have been computed using the SMIP displacement data and the interpolated displacement data for uninstrumented floors.

It is important to note that the envelopes presented are statistical estimates---associated to a 30% exceedance probability approximately, and cannot be checked with a single building point. A sufficiently large number of buildings would be necessary to describe the probability distribution for each Ω. However,

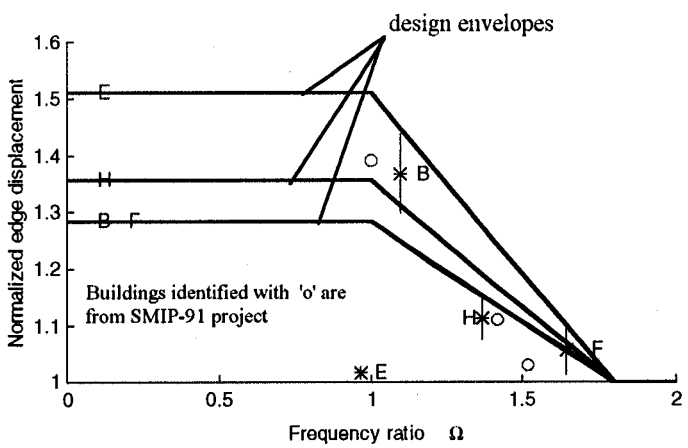

Figure 23 Increase in edge displacements, X-direction

Several observations can be obtained from these results. First, buildings with larger frequency ratios Ω present a smaller increase in displacements as predicted theoretically. It might seem contradictory that Building E presents such a small effect; however, recalling that the actual shape of the envelopes (not the simplified ones presented here) has a dip about Ω=1, this result actually agrees with theoretical predictions. Second, Building B and one of the old SMIP-91 buildings have the larger increase in edge displacements due to accidental torsion. This increase occurs for values of Ω slightly larger than one as expected analytically. It is because this sensitivity of the response around Ω=1 that the proposed design envelopes are flat at the maximum value up to this frequency ratio. Third, the vertical bars associated to each building studied denotes the heightwise variation of the increase in edge deformation. Such variability is zero only in buildings that have resisting planes with proportional stiffnesses.

ACKNOWLEDGMENTS

This investigation has been funded by the Strong Motion Instrumentation Program, California Division of Mines and Geology. The authors are grateful for this support and to Dr. Moh Huang and Dr. Gustavo Maldonado for helping in gathering all building information required during the project . Thanks are also extended to all members of the SMIP project committee for their very useful comments on the progress reports of the project.

REFERENCES

1. MATLAB, 1994. The Mathworks, Inc., Natick, Massachusetts, 1994.
2. De la Llera, J.C., and Chopra, A.K.,"Evaluation of seismic code provisions using strong-motion building records from the 1994 Northridge earthquake", CSMIP report, 1995.
3. Moehle, J., Wallace, J., and Martinez-Cruzado, J., "Implications of strong motion data for design of reinforced concrete bearing wall buildings", CSMIP Final Report, June 1990.
4. De la Llera, J.C., and Chopra, A.K., "Accidental and natural torsion in earthquake response and design of buildings", UCB/EERC-94/07, University of California, Berkeley, June 1994.